

GT2011-45- ' \$

**TWO-DIMENSIONAL NONLINEAR FINITE ELEMENT ANALYSIS OF CMC
MICROSTRUCTURES**

Subodh K. Mital

The University of Toledo
Mail Stop 49-7, NASA Glenn Research Center
Cleveland, Ohio 44135
U.S.A.

P. (216)433-3261; F. (216)433-8300; E-mail: Subodh.K.Mital@nasa.gov

Robert K. Goldberg
NASA Glenn Research Center
Mail Stop 49-7
Cleveland, Ohio 44135
U.S.A

P. 216-433-3330; F. 216-433-8300; E-mail: Robert.K.Goldberg@nasa.gov

Peter J. Bonacuse
NASA Glenn Research Center
Mail Stop 49-7
Cleveland, Ohio 44135
U.S.A

P. 216-433-3309; F. 216-433-8300; E-mail: Peter.J.Bonacuse@nasa.gov

ABSTRACT

Detailed two-dimensional finite element analyses of the cross-sections of a model CVI (chemical vapor infiltrated) SiC/SiC (silicon carbide fiber in a silicon carbide matrix) ceramic matrix composites are performed. High resolution images of the cross-section of this composite material are generated using serial sectioning of the test specimens. These images are then used to develop very detailed finite element models of the cross-sections using the public domain software OOF2 (Object Oriented Analysis of Material Microstructures). Examination of these images shows that these microstructures have significant variability and irregularity. How these variabilities manifest themselves in the variability in effective properties as well as the stress distribution, damage initiation and damage progression is the overall objective of this work. Results indicate that even though the macroscopic stress-strain behavior of various sections analyzed is very similar, each section has a very distinct damage pattern when subjected to in-plane tensile loads and this damage pattern seems to follow the unique architectural and microstructural details of the analyzed sections.

KEYWORDS

CVI, SiC/SiC Composite, Microstructure, Porosity

INTRODUCTION

High temperature ceramic matrix composites (CMC) are being explored as viable candidate materials for hot section gas turbine components, airframes and other airbreathing propulsion systems that are subjected to very high temperatures. However, these materials are heterogeneous in their make-up and various factors affect their properties in a specific design environment. Specifically, the microstructure of a woven ceramic matrix composite displays significant variability and irregularity. For example, for a CVI SiC/SiC composite, there is a significant amount of porosity arranged in irregular patterns. Furthermore, the fiber tows within a ply frequently have irregular shape and spacing, and the stacked plies are often misaligned and nested within each other. Traditional analysis methods often smear the porosity with the matrix constituent [1]. However, this can lead to incorrect prediction of composite properties, such as through-thickness modulus, where not only the amount of porosity but the shape of the porosity is also important [2]. More importantly, such traditional techniques can lack in the abilities to identify the sites for stress risers where damage is likely to initiate. Traditional techniques, where the porosity is merely smeared with the matrix or the fiber tows are regularly spaced, can only capture the stress distribution in an average sense as shown by

the authors in a previous report [1]. The goal of an ongoing project at NASA Glenn is to investigate the effects of the complex microstructure and its variability on the effective properties and the durability of the material. Detailed analysis of these complex microstructures may provide a clue to the material scientists who ‘design the material’ or to structural analysts and designers who ‘design with the material’ regarding the damage initiation and damage propagation in these materials. A model material system, specifically a five-harness satin weave architecture CVI SiC/SiC composite composed of Sylramic-iBN fibers and a SiC matrix, is analyzed. The objective is to investigate the effects of the complex microstructure on the effective mechanical properties and life, as well as to relate the microstructural variability to the variability in effective properties. A separate effort by the authors involves the development of methods to characterize the distributions in as-fabricated composites of various microstructural parameters such as tow width and spacing, ply nesting, ply misalignment etc. The variability in constituent material properties, while significant, is currently not being investigated. Towards that goal, a series of finite element analyses are performed with a simple elastic-perfectly plastic material model where 2-D cross-sections, generated from serial sectioning of experimental specimens, are subjected to an in-plane tensile load. A few computer-generated sections (also referred to as idealized or aligned) are also analyzed. The objective of this work is to perform simple progressive damage analyses on various sections to determine the sites for damage initiation, determine the sensitivity of fiber and matrix strength on the overall stress-strain behavior of the composite as well as identify the damage patterns in these sections due to in-plane tensile load and to relate the damage patterns to the unique architectural features of a given section.

MICROSTRUCTURAL CHARACTERIZATION

Samples of a representative composite specimen were serially polished and high resolution images were acquired at each polishing step. High resolution images of these polished cross-sections of the CVI SiC/SiC composite material were taken for the purposes of quantifying the distributions of various composite parameters such as: tow shape and sizes, distance between tows, size and shape of the pores, relative alignment of plies, nesting of the plies etc. The images are then segmented using an automated process that is based on pixel intensities and statistical techniques to isolate various constituents. These constituents are longitudinally sectioned tows, transverse section tows, pores and the SiC matrix surrounding the tows. However, the images of the isolated composite microstructures are not amenable to the generation of finite element models for structural analysis due to the irregular shape and sizes of constituents, ply misalignment, etc. To compensate for these irregularities, techniques were developed to generate simplified geometries from segmented images while still maintaining relevant microstructural details. This involved several approximations such as: assuming a constant thickness of the longitudinal tows based on the average values obtained from segmented images, assuming the same shape and cross-sectional area for all transverse tows, assuming a sinusoidal shape for the longitudinal tows, growing the matrix uniformly around fiber tows and slightly adjusting the position of the longitudinal and transverse tows to minimize

interference. Some ‘pristine’ or idealized sections were also generated to be used as a baseline to contrast with the more random nature of the as-manufactured composite material. As mentioned, the above technique involves some approximations that lead to differences in segmented sections and simplified section idealizations. It is observed that in actual segmented sections, matrix depositions are non-uniform; thicker on the outside and thinner in the interior. Longitudinally sectioned tows show variation in the thickness due to non-uniform cross-sectional area and slight misalignment of the plies with the sectioning plane. These and other assumptions lead to slight differences in the volume fractions of various constituents between segmented and simplified images but the overall nature of the distribution is captured. Most importantly, simplified images can be used to generate finite element models for structural analysis as explained in the following section. The details of this technique are presented in Ref. 2.

FINITE ELEMENT ANALYSIS: RESULTS

A software tool called OOF2 (Object Oriented Finite Element Analysis of Material Microstructures) [3] was used to generate finite element models from simplified images of each of the composite cross-sections generated using the serial sectioning procedure described above. This public domain software, running on any computer with a variant of the UNIX operating system, can export the finite element meshes directly into the ABAQUS general purpose finite element program [4], which can then analyze the meshes for the properties and stress distribution. Finite element meshes were created for many actual and idealized sections. A typical mesh, a finite element model of section 03, is shown in Fig. 1. The designation of section numbers is simply based on the sequence of sections taken from a test specimen of the composite.

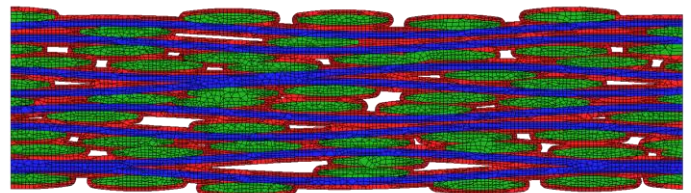


Fig.1. Finite element model of section 03 with 17442 nodes and 19502 elements (14545 linear quadrilateral and 4957 linear triangular elements)

The section consists of longitudinal (shown in blue) and transverse (shown in green) tows, CVI-matrix (shown in red) and porosity (shown as empty spaces). The longitudinal and transverse tows were treated as homogenized materials in this model even though the tow consisted of fiber, interfacial coating, matrix and intra-tow porosity. Since this intra-tow porosity is relatively uniformly distributed, this porosity was not explicitly modeled but was used in determining the homogenized properties of the tow material. In a previous report, the effective in-plane and through-thickness modulus of various sections as well as stress distributions in these sections due to an applied in-plane load were computed [2]. The idea of these analyses, performed in the linear elastic regime, was to identify the patterns of stress distribution, identify the areas of stress risers and to evaluate if any correlation could be found between the stress distribution and the composite microstructure. It was observed that the in-plane modulus

correlates very well with the amount of porosity in the section analyzed. Higher levels of porosity lead to lower values of in-plane composite modulus and show little variability. The through-thickness modulus, on the other hand, displayed a large variability as it was found to be a function of not only the amount of porosity but the shape of the porosity as well. For example, as discussed in detail in Goldberg, et al [2], for two cross-sections with equal amounts of overall porosity, when the porosity was arranged in large areas more evenly distributed throughout the cross-section, higher values of the through-thickness modulus were obtained due to the increased area of load transfer through the thickness of the composite. However, when the porosity was arranged in long thin sheets that traversed nearly the entire length of the cross-section, very low values of the through-thickness modulus were obtained due to the reduced area available for load transfer through the fiber tows. Furthermore, when the inter-tow porosity was explicitly modeled, the prediction of the through-thickness composite modulus also corresponds very well with experimentally observed values. The results also showed that if this porosity is merely smeared in the matrix, as is usually done in classical analyses, it will result in significantly higher through-thickness composite modulus than what is experimentally observed. In another study detailed in Goldberg, et al [2], since damage is likely to initiate from locations of high stresses, areas of high matrix stresses were identified and they were found to be correlated with areas where the transverse fiber tows were separated by some critical distance, as well near the area of large pores. High stress (relative to the respective strength) sites were also found in the transverse tows, mainly where the tows are closer together and thus they are also potential sites for damage initiation. Damage could initiate in transverse tows due to matrix cracking or fiber matrix debonding. It was noted that since the large irregularly shaped inter-tow porosity is explicitly modeled in these analyses (as opposed to merely smearing it with the matrix), these analyses can more accurately capture sites for high stresses and thus accurately identify sites for damage initiation. Identification of the sites of stress risers can potentially have a significant influence on the prediction of damage and life.

Following those analyses, efforts to model the progressive damage in the sections were undertaken. Damage initiation and progression models that are provided in the ABAQUS finite element program which are more appropriate for ceramic composite were tried. However, serious convergence issues were encountered and no credible answers could be obtained. While a damage mechanics type of model would be more representative of the actual material behavior, some elastic-perfectly plastic analyses were performed as a first approximation to analyze the initiation and progression of damage in the composite. A Mises yield surface that allows for isotropic yield was used for all constituents. In the future, Hill's yield surface which allows for anisotropic yield will be examined. However, due to the unidirectionally applied loads, it is not expected to make much of a difference. A strain of

0.12% in the x-direction (in-plane direction) was applied to each section analyzed at room-temperature. Table I shows the elastic properties of the fiber tows and matrix at room-temperature used in the analysis. Tow properties were computed using standard micromechanics techniques for unidirectional composites [1]. It should also be noted that since the inter-tow pores are being explicitly modeled, the bulk matrix properties are used and no calibration or in-situ effects need to be considered.

Table I. Material properties used at room-temperature

Tow Properties 800 filament Sylramic-iBN, Filament diameter = 9.5 μm , BN coating thickness = 0.6 μm , 15% porosity (assumed uniformly distributed)	EL = 260 GPa ET = 105.5 GPa LT = 0.18 GLT = 42.5 GPa
CVI-SiC Matrix	Modulus = 420 GPa Poisson's ratio = 0.2

The maximum allowable strain in the x-direction (loading direction) for each constituent was as follows: 0.06% for matrix, 0.05% for transverse tow and 0.1% for longitudinal tow based on the judgment of the authors based on representative data. This translated to a maximum allowable stress of 252 MPa (36.6 ksi) for the matrix, 260 MPa (37.6 ksi) for the longitudinal tows, and 53 MPa (7.65 ksi) for the transverse tows. The yield stress was assumed to be the failure stress or the maximum allowable stress. As mentioned earlier, post yield the constituents were assumed to be perfectly plastic. For the sake of brevity, only the results from the analysis of three sections 03, 10 (nomenclature based on the sequence of polished sections) and Ideal-01 will be presented here. The ideal section has regularly spaced tows and a very gentle undulation of longitudinal fiber tows and, in general, a very regular structure. Results show that the overall stress-strain curves of the three sections are very similar as shown in Fig. 2. No clear distinction between the material responses for each of the sections can be made at the macroscopic level.

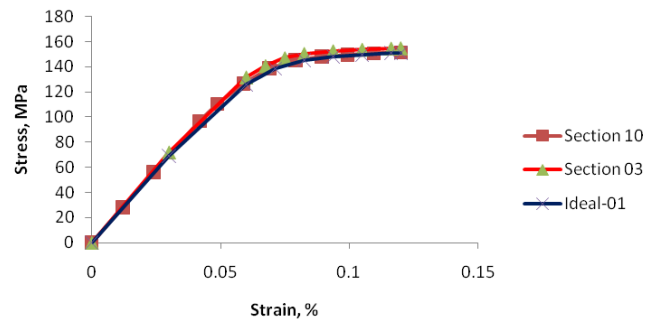


Fig. 2: Overall stress-strain curve at room-temperature for different sections

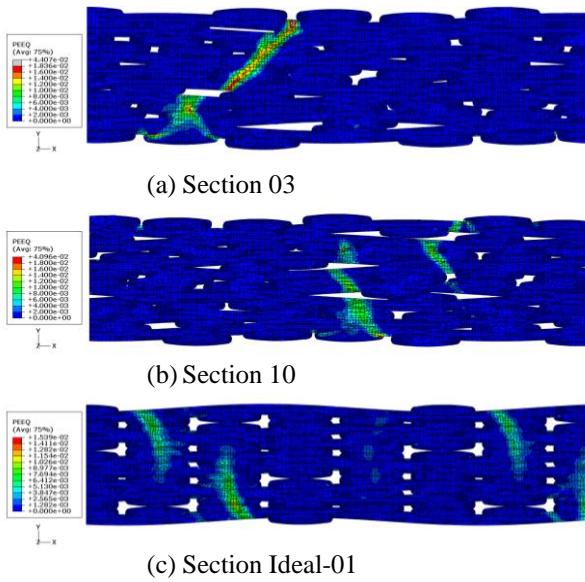


Fig. 3: Equivalent plastic strain in various sections at applied strain of 0.12% in x-direction

There is an initial elastic regime and the curve tends to deviate from the linear behavior at around 0.06% strain as shown in Fig. 2. There is a good correlation between the ‘bend-

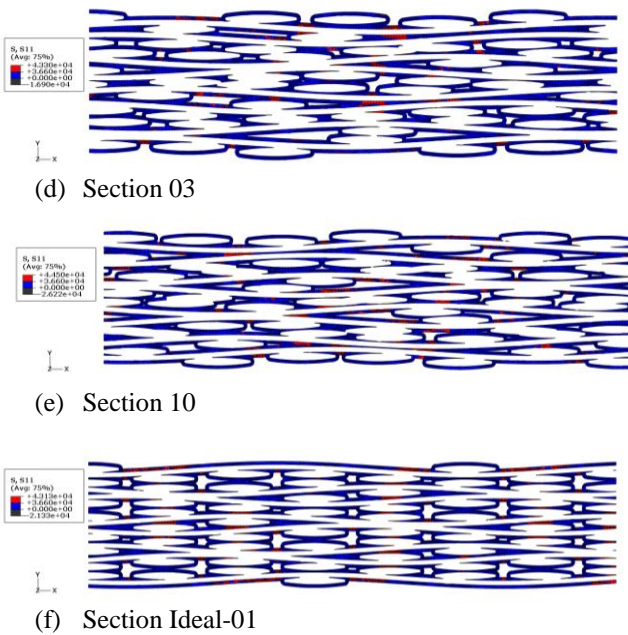


Fig. 4: Matrix damage areas, shown in red, in various sections at an applied x-strain of 0.06% (strain level at which the macro stress-strain curve starts to deviate from linear elastic behavior)

over’ point in the stress-curve shown in Fig. 2 and the experimentally observed curves, with details to be discussed

later in this report. However, the secondary part of the predicted stress-strain curve seems to be flatter than what is observed experimentally. The potential source of this difference will be discussed later. There are only slight differences in the overall volume fractions of the constituents in these sections [1]. However, the damage pattern in different sections at the applied strain of 0.12% is very different as shown in Fig. 3 and tends to follow the architectural aspects of each section analyzed, particularly in sections 3 and 10. Damage, as indicated by the presence of inelastic strains, tends to initiate from the top and bottom surface in the matrix region and the damage regions tend to connect through areas of large porosity. Fig. 4 shows the matrix damage areas (where the stress in the x-direction has reached or exceeded the allowable value) in the three sections at an applied strain of 0.06%. This is the strain value where the overall stress-strain curve starts to deviate from linear behavior; the damage in the matrix at this strain level is present in multiple localized areas. Damage tends to initiate in the matrix at the top and bottom surfaces where transverse tows are close together. Failure initiates at low strain levels and this has also been observed in experimental testing. In the ideal section, damage appears to initiate in areas near the stacked transverse tows, while in the “actual” sections the correlation between the location of the damage initiation and the local microstructure is more complex and is being investigated further. Fig. 5 shows the matrix damage areas at an applied strain of 0.12%. It shows the progression of damage is more widespread. Similar pictures of

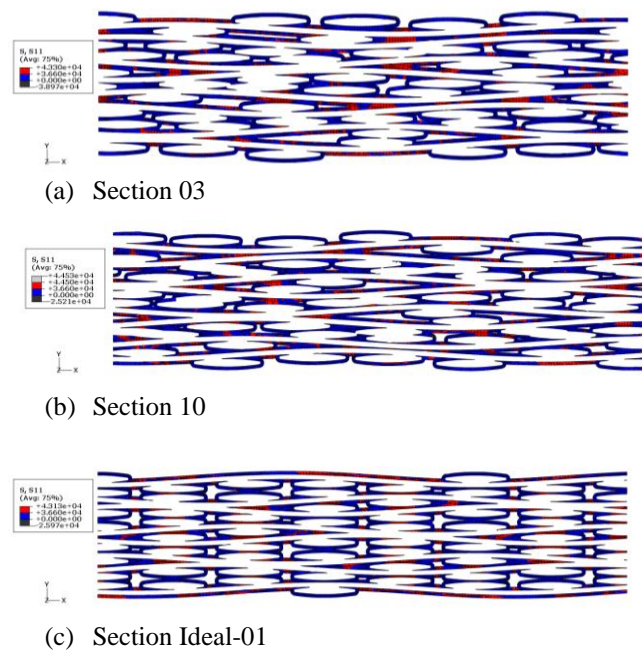


Fig. 5: Matrix damage areas, shown in red, in various sections at an applied x-strain of 0.12%

damage areas in the transverse tows are shown in Figs. 6 and 7 at applied strains of 0.06% and 0.12% respectively. Damage in the transverse tows, similar to the damage in the matrix, also appears to initiate in multiple localized areas and become more widespread at higher applied strain levels. As expected, the

idealized section shows a very regular pattern of damage initiation and progression. As with the damage in the matrix, the specific correlation between the damage patterns and the features of the microstructure are being investigated further. An important point to note is that the damage patterns shown in Figure 3 may not correlate directly with the damage patterns shown in Figures 4-7 due to the fact that the results in Figure 3 only show areas of high damage while the results in Figures 4-7 show areas where any damage (even at low levels) was

determined to have occurred.

A study was also undertaken to evaluate the effects and sensitivity of the maximum allowable strain on the overall stress-strain behavior of the composite. The maximum allowable strain of the matrix, longitudinal tows and transverse tows were changed by $\pm 25\%$ from baseline values to evaluate their sensitivity in the overall stress-strain behavior. The results from these analyses are shown in Fig. 8. As expected, the

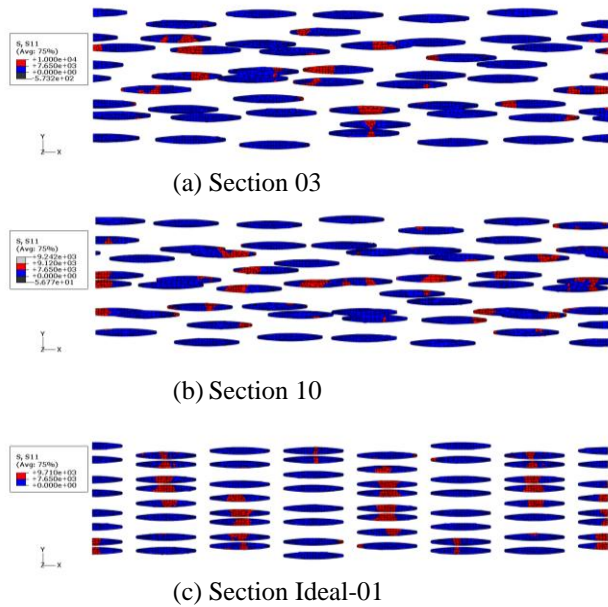


Fig. 6: Transverse tows damage areas, shown in red, in various sections at an applied x-strain of 0.06% (strain level at which the macro stress-strain curve starts to deviate from linear elastic behavior)

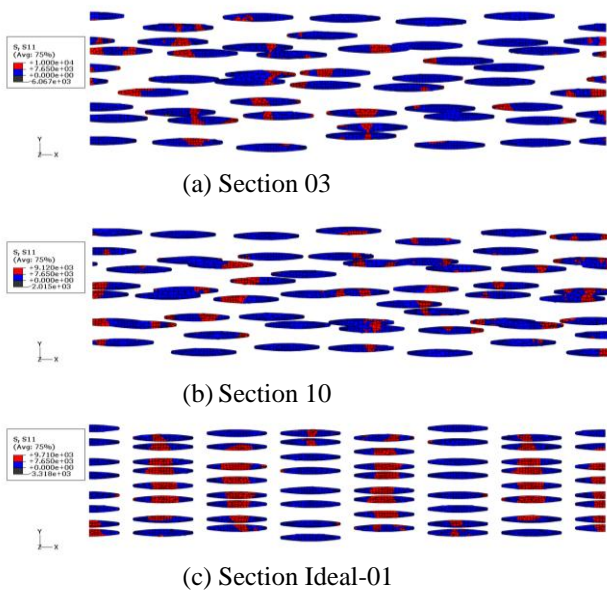


Fig. 7: Transverse tows damage areas (shown in red) in various sections at an applied x-strain of 0.12%

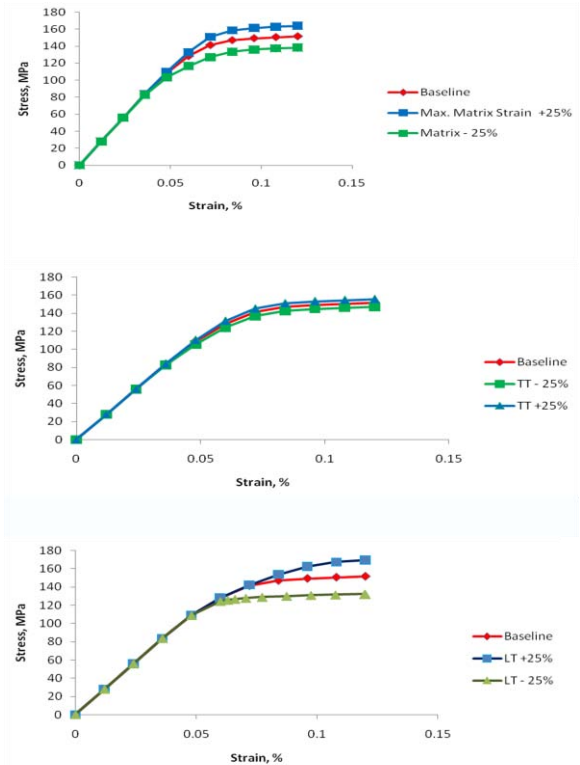


Fig. 8: Sensitivity of overall stress-strain curve of maximum allowable strain of various constituents for Section 10

results show that the matrix strength has the most influence on the ‘first matrix cracking’ stress the stress level where the curve starts to become non-linear. However, the matrix strength does not appear to have any influence on the secondary part of the stress-strain curve. The strength of the transverse tows has only a slight influence on the initiation of non-linearity as well as the secondary slope of the overall stress-strain curve. The strength of the longitudinal tows has little or no influence on the initiation of the non-linearity in the stress-strain curve, but it has a significant influence on the secondary part of the stress-strain behavior. Since the maximum allowable strain level of 0.1% was considered to be too low for the longitudinal tows, the sensitivity of this assumed value is also shown in Fig. 9. Results shown in this figure indicate that the longitudinal tow strength has a major influence on the secondary slope of the overall composite and for the most part controls the ultimate failure. The maximum allowable strain in the longitudinal tows

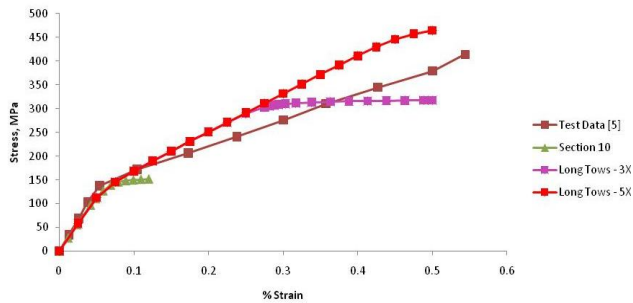


Fig. 9: Sensitivity of overall stress-strain curve with longitudinal tow strength, comparison with some test data is also shown

appears to be closer to 0.5%, the overall composite failure strain, much higher than the value previously assumed in the analyses. Overall, the results show that even with the simple damage (elastic perfectly-plastic) model, the predicted stress-strain behavior is able to at least qualitatively capture the material response and is able to capture the important aspects of the overall stress-strain behavior. Comparison with available test data is also reasonable as shown in Fig. 9.

SUMMARY/CONCLUSIONS

Detailed finite element analyses of a model material system, specifically a five-harness 2-D satin weave architecture CVI SiC/SiC composite were performed. Since these composites display significant irregularity and variability in their microstructure, this work sought to evaluate the effect of this variability on overall composite properties and damage initiation and progression leading to failure. Results indicate that even though the overall macroscopic behavior of the composite is not different between various sections despite the difference in microstructure composition, the damage pattern is

very different in each section. It appears to follow the architectural and microstructural details of the sections analyzed. Even a simple damage (elastic perfectly-plastic) model is able to capture the overall behavior as well as the damage initiation sites and progression that is in good agreement with the test data. Future work will involve analyzing more realistic sections such as with varying matrix thickness, using more realistic damage models suitable for ceramic materials, further investigation of the effects of microstructural features on damage and link to actual material variability as well as developing scaling laws to link effects of microstructure to continuum level analysis.

REFERENCES

- [1] Mital, S.K.; Bednarczyk, B.A. et. al: Modeling of Melt-Infiltrated SiC/SiC Composite Properties. NASA Technical Memorandum, NASA/TM-2009-215806, October 2009.
- [2] Goldberg, R. K.; Bonacuse, P. J.; and Mital, S. K.: "Investigation of Effects of Material Architecture on the Elastic Response of a Woven Ceramic Matrix Composite," NASA Technical Memorandum – in preparation.
- [3] Reid, A. et. al.: "Modeling Microstructures with OOF2", Int. J. Materials and Product Technology, Vol. 35, pp. 361-373, 2009.
- [4] ABAQUS General Purpose Finite Element Program. Version 6.8, SIMULIA, Providence, RI
- [5] Kiser, J; Calomino, A.; et. al: SiC/SiC Composites for High Temperature Applications. Proc. of HTCMC-7 (7th International Conference on High Temperature Ceramic Matrix Composites), Sept. 19-22, 2010, Bayreuth, Bavaria, Germany.